



1 Diurnal cycle of clouds extending above the tropical tropopause
2 observed by spaceborne lidar

3 Dauhut, Thibaut (1), Vincent Noel (2) and Iris-Amata Dion (3)

4 1. Max Planck Institute for Meteorology, Hamburg, Germany

5 2. Laboratoire d'Aérodynamique, Université de Toulouse, CNRS, UPS, Toulouse, France

6 3. CRNM, Météo-France – CNRS, Toulouse, 31057, France

7 Proposed for publication in Atmospheric Chemistry and Physics

8 Contact author : T. Dauhut thibaut.dauhut@mpimet.mpg.de

9 Abstract

10 The presence of clouds above the tropopause over tropical convection centers has so far been
11 documented by spaceborne instruments that are either sun-synchronous, or insensitive to thin
12 cloud layers. Here we document, for the first time through direct observation by spaceborne lidar,
13 how the tropical cloud fraction evolves above the tropopause throughout the day. After confirming
14 previous studies that found such clouds are most frequent above convection centers, we show that
15 stratospheric clouds and their vertical extent above the tropopause follow a diurnal rhythm linked
16 to convective activity. The diurnal cycle of the stratospheric clouds displays two maxima: one in the
17 early night (19-20LT) and a later one (00-01LT). Stratospheric clouds extend up to 0.5-1km above
18 the tropopause during nighttime, when they are the most frequent. The frequency and the vertical
19 extent of stratospheric clouds is very limited during daytime, and when present they are found
20 very close to the tropopause. Results are similar over the major convection centers (Africa, South
21 America, Warm pool), with more clouds above land in DJF and less above ocean and JJA.



22 1. Scientific context and objectives

23 The presence of ice clouds near the tropical tropopause has long been documented by in-situ
24 measurements (e.g. Thomas et al., 2002; Jensen et al., 2013; Frey et al., 2014). Detecting
25 occurrences of clouds extending above the tropopause by remote sensing requires documenting
26 the vertical cloud profile with a fine resolution and a high sensitivity to optically thin clouds, which
27 few instruments can reach. Lidar measurements are able to document such occurrences (e.g. Nee
28 et al., 1998), but for a long time were limited to local case studies. Dessler (2009) was the first to
29 use the cloud detections by the CALIPSO lidar (Cloud-Aerosol Lidar Infrared Pathfinder Satellite
30 Observations) to investigate how clouds extend above the tropopause on a global scale. Pan and
31 Munchak (2011) refined the results by using an advanced tropopause dataset. Both studies found
32 that clouds extending into the stratosphere are frequent above seasonal deep convection centers
33 and rarely elsewhere, especially in midlatitudes. Both studies deplored that the fixed overpass
34 local time of the CALIPSO dataset is far from the late afternoon, when land convection is at its
35 maximum. More recently, Wang et al. (2019) documented the presence of laminar cirrus in 10
36 years of CALIPSO data, and reported a non-negligible cloud amount above the tropopause.
37 Because of the sun-synchronous orbit of CALIPSO, none of these studies were able to document
38 the diurnal cycle of the stratospheric clouds.

39 Low-stratospheric clouds impact the atmospheric system in several ways. First, their larger heating
40 rate than the clear sky (Corti et al, 2006) increases the upward mass flux and fosters the large-scale
41 upward transport of water above the tropopause. At the hour timescale, the cloud particles
42 penetrating the stratosphere via overshooting convection leads, on the one hand, to a direct
43 stratospheric humidification (Schoeberl et al., 2018; Dauhut et al., 2018). On the other hand, these
44 particles can serve as support for ice-scavenging: under saturated conditions, the water vapor
45 deposits on the particles, which grow and fall out (Corti et al., 2008), decreasing low-stratosphere
46 humidity (Jensen et al., 2013). By all these effects the stratospheric clouds modulate the



48 stratospheric water vapor concentrations (Iwasaki et al., 2015) and affect the overall dynamical
49 structure near the tropopause (Corti et al., 2006), at timescales down to one hour. This is why it is
50 important to understand the formation and the sub-daily evolution of such clouds.

51 Finding the processes responsible for the formation of tropical stratospheric clouds proves difficult,
52 just like with high-tropospheric clouds (Reverdy et al., 2012). Two processes have been mainly
53 proposed. Overshooting convection can lead to the injection of ice crystals into the stratosphere
54 (Dauhut et al., 2018; Lee et al., 2018). Stratospheric cooling triggered by gravity waves (Pfister et
55 al., 2010) could also lead to so-called cloud “in-situ” formation (Pan and Munchak, 2011). The ratio
56 of stratospheric clouds that are formed in-situ has not been estimated yet. The current study does
57 not provide further estimate, but by describing the spatio-temporal evolution of the stratospheric
58 clouds, it highlights how important the convective activity is to drive the stratospheric cloudiness,
59 and how the twice-daily sampling by lidars onboard sun-synchronous platforms can miss the
60 highest and largest stratospheric cloud fraction over certain regions.

61 In this paper, we document for the first time the diurnal cycle of clouds above the tropopause in
62 the Tropics, and the extent of their penetration in the stratosphere, thanks to the high vertical and
63 temporal resolution of the cloud detection by the CATS (Cloud-Aerosol Transport System)
64 spaceborne lidar (McGill et al., 2015). After describing CATS cloud data, and the method to retrieve
65 the tropopause heights used to detect clouds extending in the stratosphere (Sect. 2), we present
66 maps of stratospheric clouds and document their diurnal cycle in regions of interest (Sect. 3). We
67 then summarise our results and conclude (Sect. 4).



68 2. Data and Methods

69 2.1 CATS Cloud data

70 The CATS lidar operated from the International Space Station (ISS) between February 2015 and
71 November 2017. It reported profiles at a vertical resolution of 60m every 350m along-track, with
72 an average repeat cycle of nearly 3 days (Yorks et al., 2016). Thanks to the ISS non-synchronous
73 orbit, CATS was able to probe the vertical cloud distribution of a particular region at different times
74 of the day. Aggregating CATS detections over a region of interest and over enough time provides a
75 statistical overview of the diurnal evolution of cloud vertical profiles over that region (Noel et al.,
76 2018).

77 CATS Level 2 Operational layer files (L2O files, Palm et al., 2016) describe altitudes where cloud
78 layers were detected within profiles of backscatter coefficients measured at 1064nm by the CATS
79 lidar (Pauly et al., 2019), averaged 5km along-track. We considered all such files over the CATS
80 operation period (February 2015 to November 2017) and inspected each 5-km profile within. For
81 profiles located in the Tropics (30S-30N), we inspected each atmospheric layer therein identified as
82 a cloud layer according to the CATS layer type information. As in Noel et al. (2018), we considered
83 layers with a Feature Type Score above 6, to avoid any possibly mislabeled aerosol layers. We
84 flagged the cloud layers with a top altitude above the tropopause. Since any CATS L2O layer
85 entirely above the tropopause is labelled as an aerosol layer (like in CALIPSO, Pan and Munchak,
86 2011), our study will not include clouds with their base in the stratosphere.

87 Davis et al (2010) noted that lidars in space may miss the thinnest subvisible cirrus clouds, but with
88 enough spatial averaging optical depths near 0.001 can be detected (Martins et al., 2011). Lidar
89 cloud detections also suffer from a lower sensitivity in the presence of sunlight, which induces
90 significant additional noise in the lidar signal, but climatologies are still relevant (Noel et al., 2018).



91 2.2. Tropopause Heights

92 To obtain the tropopause height, we considered profiles of temperature and pressure from the
93 ERA-5 reanalysis dataset (Albergel et al., 2018). These profiles are available every 6 hours, on 37
94 vertical levels and a $0.25^\circ \times 0.25^\circ$ horizontal grid. Such profiles in ERA-5 reanalysis agree well with
95 observations in the high tropical troposphere (Podglajen et al. 2014). Using these profiles, we
96 computed the vertical lapse rate profile (as in Reichler et al. 2003), and interpolated it on a 100-m
97 vertical grid. We then applied the WMO criteria defining the presence of a tropopause -- i.e. the
98 lowest altitude at which the lapse rate falls below $2^\circ\text{C}/\text{km}$, provided the lapse-rate between this
99 level and all higher levels within 2 km does not exceed $2^\circ\text{C}/\text{km}$ (WMO, 1957). Following the WMO
100 definition, we also allowed for the possibility of a second tropopause if the lapse rate exceeds
101 $3^\circ\text{C}/\text{km}$ at least 1 km above the first tropopause. In such a case, we started to look for another
102 tropopause above. To limit computation overhead we constrained the search below 22 km. Using
103 the WMO tropopause definition further allows us to compare our results to previous efforts based
104 on CALIPSO database that used the same definition (Pan and Munchak, 2011).

105 2.3 Stratospheric cloud detection

106 For a given CATS 5-km profile (Sect. 2.1), we identified the ERA-5 tropopause height (Sect. 2.2)
107 closest in time and location. Given the 6-hour time resolution of the ERA-5 reanalysis, there is at
108 most 3 hours difference between the observation time and the thermodynamic information used
109 to retrieve the tropopause height. We used the cloud information contained in the 5-km profiles in
110 two ways. First, in $2^\circ \times 5^\circ$ lat-lon bins we counted how many profiles contained a cloud extending
111 above the tropopause, compared to the total number of profiles in the bins. Aggregating such
112 numbers observed in JJA and DJF over the CATS operation period produced seasonal maps of
113 above-tropopause cloud amounts (Sect. 3.1). Second, from each CATS 5-km profile we built a



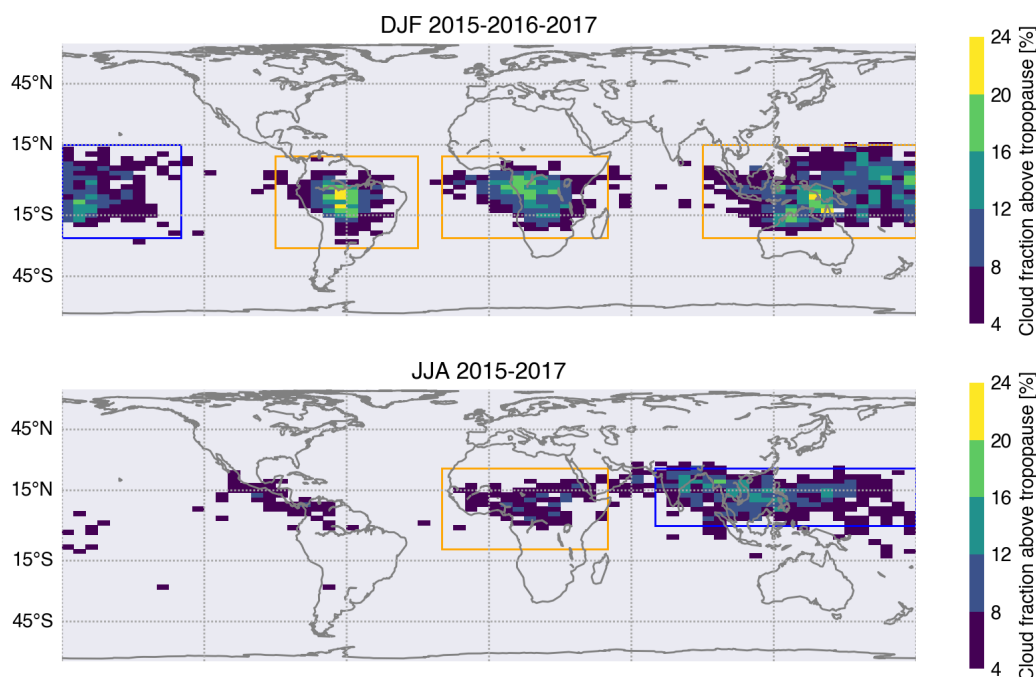
114 vertical cloud mask, using the tropopause height as the vertical reference and considering clouds
115 that extend above it. Within regions chosen based on the seasonal maps, we aggregated such
116 cloud masks over the same periods as above, keeping also track of the local time of observation for
117 the considered mask. This produced regional vertical cloud fraction profiles above the tropopause,
118 one profile for each local time of observation (Sect. 3.2).



119 3. Results

120 3.1 Stratospheric cloud distributions

121 Figure 1 shows the fraction of CATS profiles in which a cloud is detected above the tropopause, in
122 all DJF (top) and JJA (bottom) months of CATS operation.



123 **Figure 1:** Tropical low-stratosphere cloud fraction for (top) DJF and (bottom) JJA CATS
124 measurements between Feb 2015 and Nov 2017, calculated by considering all profiles in $2^\circ \times 5^\circ$ lat-
125 lon boxes. The rectangles are the regions in which cloud detections are aggregated in the rest of
126 the study. In DJF, from left to right : West Pacific (25S-15N, 180W-130W), South America (30S-10N,
127 90W-30W), Equatorial Africa (25S-10N, 20W-50E), and South Warm Pool (25S-15N, 90E-180E). In
128 JJA, from left to right : Central Africa (10S-25N, 20W-50E), North Warm Pool (0-25N, 70E-180E).
129 Only detections in the $\pm 30^\circ$ region are shown here. In the rest of the study, we considered profiles
130 over ocean in blue boxes and profiles over land in orange boxes.

131 Figure 1 shows that clouds in the tropical stratosphere are mostly detected over continents (South
132 America, Equatorial Africa and land masses in South Warm Pool in DJF; Central America, Central
133 Africa and land masses in North Warm Pool in JJA). The cloud fraction in the lower stratosphere is



134 largest in DJF, up to 24% over central Amazonia and coastal areas in South Warm Pool, and up to
135 20% over Equatorial Africa. It is significantly lower in JJA, up to 12% over Africa and 16% over the
136 North Warm Pool, even though the lowermost stratosphere (380-420 K potential temperature) is
137 moister in JJA than in DJF (cf. e.g. Fig. 8c in Fueglistaler et al, 2009). Several factors may contribute
138 to this seasonal variation: the density and strength of the convective systems (Liu and Zipser,
139 2005), their propensity to propagate or to be stationary (Houze et al, 2015), the activity and
140 efficiency of the in situ formation processes (Jensen et al., 2001; Jensen and Pfister, 2004).

141 The spatio-temporal distribution of the stratospheric clouds is in very good agreement with the 4-
142 year climatology of Pan and Munchak (2011) from CALIPSO observations. The DJF distribution also
143 matches very well the CALIOP cirrus detection at 100 hPa reported by Wang et al (2019) for
144 January 2009. We report though lower cloud frequencies than Wang et al. (2019) which can be
145 explained that we investigate slightly higher levels. Both CATS and CALIPSO datasets find 1)
146 significantly weaker stratospheric cloud fraction in JJA than in DJF, and 2) near-zero stratospheric
147 clouds in the subtropics. These results are also consistent with the CALIPSO cloud fractions near
148 16km reported by Schoeberl et al. (2019). Since those studies consider cloud detections derived
149 from a spaceborne lidar instrument, over several years for most, their good agreement suggests
150 that the CATS stratospheric cloud detections at 1064 nm are as reliable as the CALIPSO ones at 532
151 nm. A first conclusion of our results is therefore that CATS measurements strongly support the
152 findings of all other studies using detections of high clouds from CALIPSO data.

153 Comparing our CATS results to the distributions of clouds at 90 hPa/17 km retrieved from HIRDLS
154 and CALIPSO for 2006-2007 by Massie et al. (2010), we also find good agreement in JJA but larger
155 differences in DJF. In CALIPSO and HIRDLS, the maxima are over the West-to-Central Pacific and the
156 convective spot in South America is shifted West towards the Pacific. This difference can be
157 explained by the annual variability: in DJF 2006-2007 the Southern Oscillation Index indicates



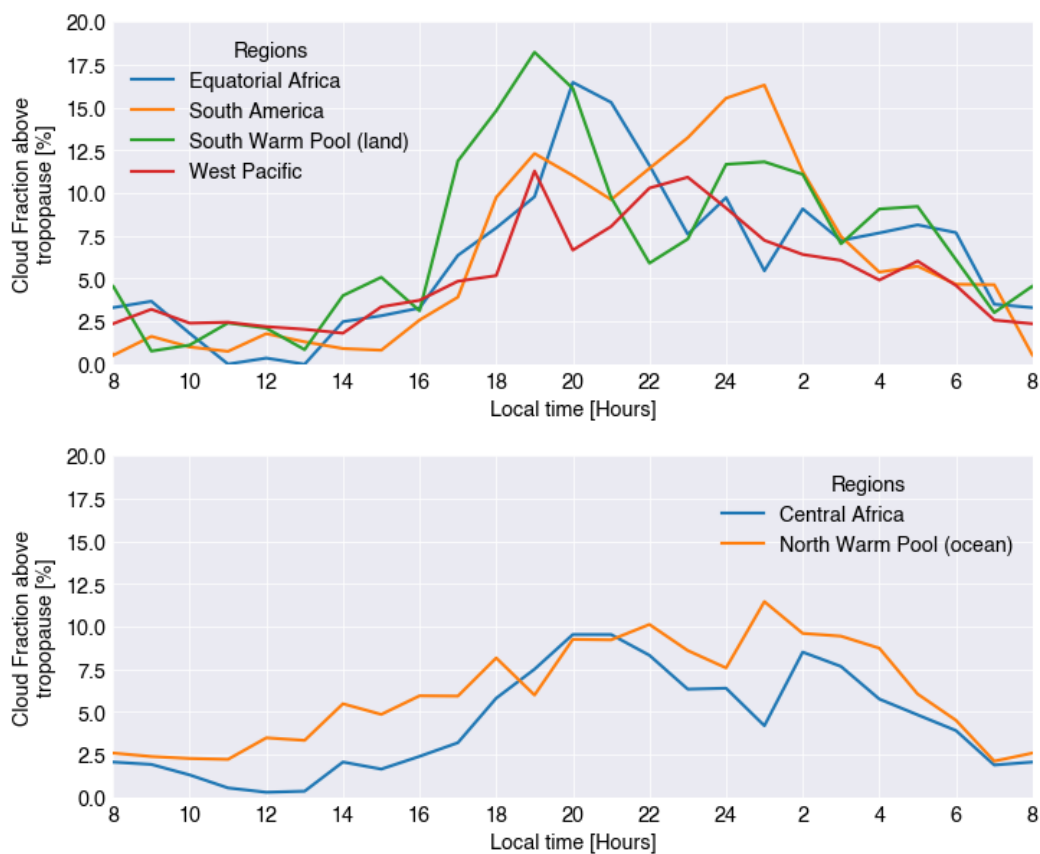
158 rather El-Nino conditions, like in DJF 2015-2016 but in contrast with DJF 2016-2017, both being
159 included in our study.

160 Our results match the overall distributions of cloud tops higher than 17 km retrieved from
161 CloudSat 8-year observations by Kim et al. (2018). In particular, the Warm Pool exhibits the largest
162 area with significant stratospheric cloud fraction, both during DJF and JJA. Little differences
163 between CATS and CloudSat data sets appear in DJF: in the CATS dataset the South America show
164 slightly larger cloud fraction than the Equatorial Africa; in the CloudSat dataset, the largest cloud
165 fractions over Africa are located more south-east (Great Lakes and Madagascar straight). Note that
166 the CloudSat radar samples convection at 1:30 am and pm, potentially missing some continental
167 convective systems. These differences might also be due to the different periods considered: 2006-
168 2014 for CloudSat versus 2015-2017 for CATS. On the contrary, our results contrast with Liu and
169 Zipser (2005) distributions derived from the TRMM Precipitation Radar, where the densities of
170 overshooting systems with tops in the lower stratosphere are remarkably larger in Central America
171 and Central Africa than over the Warm Pool. Since TRMM precipitation radar reflectivities are less
172 sensitive to thin ice particles than CATS and CALIOP lidars, we can interpret this difference by the
173 fact that the American and African systems, though frequently overshooting the stratosphere,
174 produce less stratospheric clouds than the Asian systems.

175 Finally, our results agree well with the pioneering work of Jensen et al. (1996) who used passive
176 SAGE II observations at 17.5 km for 1989: their cloud fractions are larger because the considered
177 level is closer to the cold point tropopause but the geographical distributions are very close to
178 ours. The differences are: in DJF they observe more clouds over the Atlantic but less over South
179 America, in JJA they observe less clouds over the West Pacific. These differences may be due to the
180 year-to-year variability. The SAGE II instrument relies on a solar occultation method, completely
181 different from the active lidar observation by CATS and CALIPSO.



182 **3.2 Diurnal cycle of cloud fractions in the tropical stratosphere**

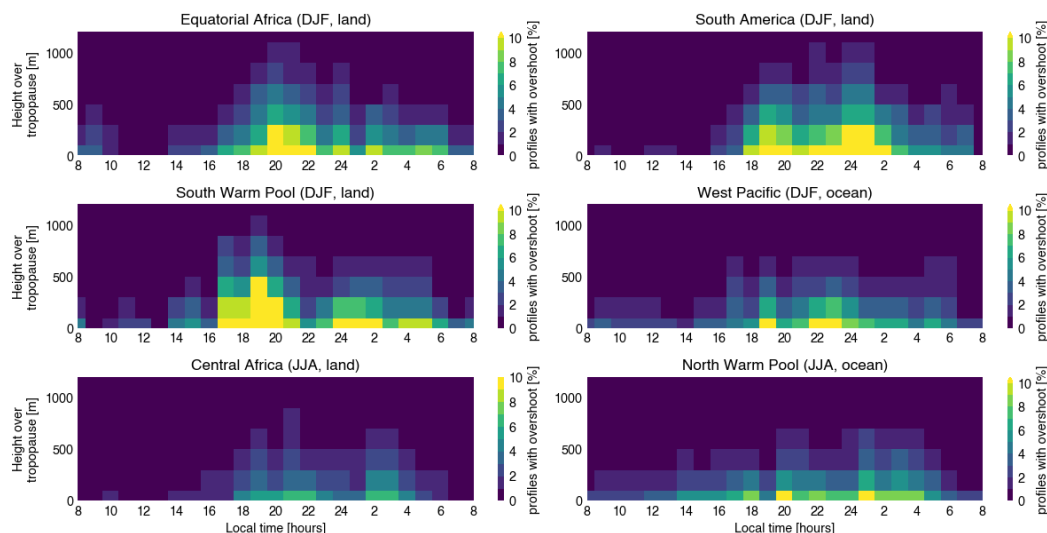


183 **Figure 2:** Diurnal cycle of stratospheric cloud fraction, by tropical region as in Fig. 1, averaged over
184 DJF (top) and JJA (bottom).

185 In contrast with the previous studies, the CATS dataset allows us to analyse the diurnal cycle of the
186 cloud fraction in stratosphere. The cloud fraction at regional scale shows a consistent diurnal cycle,
187 robust over the different regions identified in the previous section (Fig. 2). In particular and in
188 contrast to the diurnal cycle of surface precipitation, there is no land-ocean difference. All exhibit a
189 pronounced minimum about 2-4 % during the day time, from 7 to 16 LT. They all present a first
190 maximum at 19 or 20 LT (early-night peak), up to 18% over South Warm Pool; over North Warm
191 Pool this peak is slightly later. For all regions except South America, this maximum is the largest



192 cloud fraction of the day. All regions also present a secondary peak at 0 or 1 LT (2 LT for Central
193 Africa), up to 16% over South America.



194 **Figure 3:** Diurnal cycle of cloud fraction as a function of height above the tropopause, by tropical
195 region as in Fig. 1, in DJF (top 2 rows) and JJA (bottom row).

196 Figure 3 shows how far above the tropopause the clouds extend, depending on the local time in
197 each tropical region (Sect. 3.1). Some regions are considered in DJF, others in JJA, because the
198 stratospheric cloud distribution changes throughout the year (Fig. 1), following the ITCZ position.
199 Patterns appear very consistent in all the regions considered. In all regions the largest cloud
200 fractions are found near the tropopause, with few clouds extending higher. Cloud fractions extend
201 relatively high (up to 1km above the tropopause) during the early night. The first peak of cloud
202 fraction, near 19-20LT (Fig. 2), is associated with the all-day maximum of cloud vertical extent, with
203 clouds in 5% of profiles reaching 1km above the tropopause in DJF regions. During the rest of the
204 night (after 00 LT) clouds are still present but extend less high. During daytime (0600-1800) clouds
205 appear very close to the tropopause. Cloud fractions are overall much smaller in JJA (max 5-10%,
206 bottom row) than in DJF (max 10-12%, rows 1 and 2).



207 In addition to describing the evolution of the stratospheric cloud cover at hourly timescales, these
208 observations help interpret observations with limited temporal sampling (Noel et al., 2018). The
209 Microwave Limb Sounder (MLS), like CALIPSO and all other instruments onboard platforms of the
210 A-Train, samples the atmosphere at 01:30 and 13:30 LT, providing one single night and one single
211 day observation. Some authors (e.g., Dion et al., 2019) attempt to retrieve the diurnal cycle of the
212 observed water contents in the tropopause region, combining MLS observations with higher
213 temporal resolution observation of convective activity based on TRMM observation of
214 precipitation. Dion et al. (2019) assumed an in-phase relationship between precipitation and ice
215 water content in the upper troposphere and at the tropopause level. For the stratospheric ice
216 water content, MLS data still provides a too low signal-to-noise ratio. For future investigations, our
217 results indicate that the stratospheric cloud fraction at 13:30 LT is, whatever the region, close to
218 the minimal value of its diurnal cycle, whereas at 01:30 LT it is more typical of the secondary
219 maximum. Carminati et al. (2014) investigated, from MLS measurements between 2005 and 2012,
220 the differences between day and night ice water contents in the upper troposphere and the
221 tropopause level. Unlike the stratospheric cloud fraction, tropopause ice water contents are larger
222 at 13:30 LT than at 01:30 LT over Equatorial Africa during DJF, Central Africa during JJA, and over
223 South America during both seasons. A possible explanation to reconcile our results is that
224 tropopause ice water content is more sensitive to fresh convective activity (very deep convection
225 occurrence) whereas the stratospheric cloud cover is more sensitive to the diffusion of the injected
226 ice in the stratosphere.



227 4. Conclusion

228 Our results show how clouds in the tropical stratosphere are strongly concentrated above deep
229 convection centers, are almost absent in subtropical regions, are more frequent in DJF than JJA,
230 and over land than over ocean. In addition to these results, which are consistent with most
231 previous studies, we also show that both the cloud fraction and its extension above the
232 tropopause follow a diurnal rhythm with a maximum during the early nighttime and a near-zero
233 minimum during daytime. During daytime, the stratospheric clouds are limited to the first hundred
234 meters above the tropopause. During nighttime, significant average cloud fraction is found up to 1
235 km above the tropopause. A secondary maximum of stratospheric cloud fraction is observed over
236 all regions, generally little after midnight. Further investigation is necessary to identify the
237 processes driving this diurnal cycle, and leading in particular to the minimal stratospheric cloud
238 fraction during daytime and the secondary peak during nighttime, both consistent over all regions.
239 Finally further research is needed to understand why the timing of this diurnal cycle is very similar
240 over land and over ocean.

241 **Author contribution.** TD and VN designed the data analyses and VN carried them out. TD
242 prepared the manuscript with contributions from VN and ID.

243 **Acknowledgments.** The authors would like to thank B. Legras (LMD) and F. Pantillon (LA) for
244 useful discussions on the quality of tropopause altitudes from various sources. They also thank
245 NASA EarthData for access to CATS data and ECMWF for access to the ERA5 reanalysis dataset. This
246 research was supported by the IDEX TEASAO project. Primary data and scripts used in the analysis
247 and other supplementary information that may be useful in reproducing the author's work are
248 archived by the Max Planck Institute for Meteorology and can be obtained by contacting
249 publications@mpimet.mpg.de



250 References

- 251 • Albergel, C., Dutra, E., Munier, S., Calvet, J.-C., Munoz-Sabater, J., de Rosnay, P., and
252 Balsamo, G.: ERA-5 and ERA-Interim driven ISBA land surface model simulations: which one
253 performs better?, *Hydrol. Earth Syst. Sci.*, 22, 3515-3532, [https://doi.org/10.5194/hess-22-](https://doi.org/10.5194/hess-22-3515-2018)
254 [3515-2018](https://doi.org/10.5194/hess-22-3515-2018), 2018.
- 255 • Carminati, F., Ricaud, P., Pommereau, J.-P., Rivière, E., Khaykin, S., Attié, J.-L., and Warner, J.:
256 Impact of tropical land convection on the water vapour budget in the tropical tropopause
257 layer, *Atmos. Chem. Phys.*, 14, 6195-6211, <https://doi.org/10.5194/acp-14-6195-2014>,
258 2014.
- 259 • Corti, T., Luo, B. P., Fu, Q., Vömel, H., and Peter, T.: The impact of cirrus clouds on tropical
260 troposphere-to-stratosphere transport, *Atmos. Chem. Phys.*, 6, 2539-2547,
261 <https://doi.org/10.5194/acp-6-2539-2006>, 2006.
- 262 • Corti, T., et al.: Unprecedented evidence for deep convection hydrating the tropical
263 stratosphere, *Geophys. Res. Lett.*, 35, L10810, <https://doi.org/10.1029/2008GL033641>,
264 2008.
- 265 • Dauhut, T., Chaboureaud, J., Haynes, P.H., and Lane, T.P.: The Mechanisms Leading to a
266 Stratospheric Hydration by Overshooting Convection, *J. Atmos. Sci.*, 75, 4383-4398,
267 <https://doi.org/10.1175/JAS-D-18-0176.1>, 2018.
- 268 • Davis, S., et al.: In situ and lidar observations of tropopause subvisible cirrus clouds during
269 TC4, *J. Geophys. Res.*, 115, D00J17, <https://doi.org/doi:10.1029/2009JD013093>, 2010.
- 270 • Dessler, A. E.: Clouds and Water Vapor in the Northern Hemisphere Summertime
271 Stratosphere, 114, *J. Geophys. Res.*, 114, <https://doi.org/10.1029/2009JD012075>, 2009.
- 272 • Dion, I. A., Ricaud, P., Haynes, P., Carminati, F., and Dauhut, T.: Ice injected into the
273 tropopause by deep convection – Part 1: In the austral convective tropics, *Atmos. Chem.*
274 *Phys.*, 19(9), 6459-6479, <https://doi.org/10.5194/acp-19-6459-2019>, 2019.
- 275 • Frey, W., Borrmann, S., Fierli, F., Weigel, R., Mitev, V., Matthey, R., Ravegnani, F., Sitnikov, N.
276 M., Ulanovsky, A., and Cairo, F.: Tropical deep convective life cycle: Cb-anvil cloud



- 277 microphysics from high-altitude aircraft observations, *Atmos. Chem. Phys.*, 14, 13223-
278 13240, <https://doi.org/10.5194/acp-14-13223-2014>, 2014.
- 279 • Houze, R. A., Rasmussen, K. L., Zuluaga, M. D., and Brodzik, S. R.: The variable nature of
280 convection in the tropics and subtropics: A legacy of 16 years of the Tropical Rainfall
281 Measuring Mission satellite, *Rev. Geophys.*, 53, 994–1021,
282 <https://doi.org/10.1002/2015RG000488>, 2015.
- 283 • Iwasaki, S., Luo, Z. J., Kubota, H., Shibata, T., Okamoto, H., and Ishimoto, H.:
284 Characteristics of cirrus clouds in the tropical lower stratosphere, *Atmos. Res.*, 164–165,
285 358–368, <https://doi.org/10.1016/j.atmosres.2015.06.009>, 2015.
- 286 • Jensen, E. J., Toon, O. B., Selkirk, H. B., Spinhirne, J. D., and Schoeberl, M. R.: On the
287 formation and persistence of subvisible cirrus clouds near the tropical tropopause, *J.*
288 *Geophys. Res.*, 101(D16), 21361– 21375, <https://doi.org/10.1029/95JD03575>, 1996.
- 289 • Jensen, E. J., Pfister, L., Ackerman, A. S., Tabazadeh, A., and Toon, O. B.: A conceptual model
290 of the dehydration of air due to freeze-drying by optically thin, laminar cirrus rising slowly
291 across the tropical tropopause, *J. Geophys. Res.*, 106(D15), 17237– 17252,
292 <https://doi.org/10.1029/2000JD900649>, 2001.
- 293 • Jensen, E., and Pfister, L.: Transport and freeze-drying in the tropical tropopause layer, *J.*
294 *Geophys. Res.*, 109, D02207, <https://doi.org/10.1029/2003JD004022>, 2004.
- 295 • Jensen, E. J., Diskin, G., Lawson, R. P., Lance, S., Bui, T. P., Hlavka, D., McGill, M., Pfister, L.,
296 Toon, O. B., and Gao, R.: Ice nucleation and dehydration in the Tropical Tropopause Layer,
297 *PNAS*, 110, 2041–2046, doi:10.1073/pnas.1217104110, 2013.
- 298 • Kim, J., Randel, W. J., and Birner, T.: Convectively driven tropopause-level cooling and its
299 influences on stratospheric moisture, *J. Geophys. Res.-Atmos.*, 123, 590– 606,
300 <https://doi.org/10.1002/2017JD027080>, 2018.
- 301 • Lee, K.-O., Dauhut, T., Chaboureaud, J.-P., Khaykin, S., Krämer, M., and Rolf, C.: Convective
302 hydration in the tropical tropopause layer during the StratoClim aircraft campaign: Pathway
303 of an observed hydration patch, *Atmos. Chem. Phys. Discuss.*, [https://doi.org/10.5194/acp-](https://doi.org/10.5194/acp-2018-1114)
304 [2018-1114](https://doi.org/10.5194/acp-2018-1114), preprint, 2018.



- 305 • Liu, C., and Zipser, E. J.: The global distribution of largest, deepest, and most intense
306 precipitation systems, *Geophys. Res. Lett.*, 42, 3591– 3595,
307 <https://doi.org/10.1002/2015GL063776>, 2005.
- 308 • Martins, E., Noel, V., and Chepfer, H.: Properties of cirrus and subvisible cirrus from
309 nighttime Cloud-Aerosol Lidar with Orthogonal Polarization (CALIOP), related to
310 atmospheric dynamics and water vapor, *J. Geophys. Res.*, 116, D02208,
311 <https://doi.org/10.1029/2010JD014519>, 2011.
- 312 • Massie, S. T., Gille, J., Craig, C., Khosravi, R., Barnett, J., Read, W., and Winker, D.: HIRDLS
313 and CALIPSO observations of tropical cirrus, *J. Geophys. Res.*, 115, D00H11,
314 <https://doi.org/10.1029/2009JD012100>, 2010.
- 315 • McGill, M. J., Yorks, J. E., Scott, V. S., Kupchock, A. W., and Selmer, P. A.: The Cloud-Aerosol
316 Transport System (CATS): A technology demonstration on the International Space Station,
317 *Proc. SPIE 9612, Lidar Remote Sensing for Environmental Monitoring XV*, 96120A,
318 <https://doi.org/10.1117/12.2190841>, 2015.
- 319 • Nee, J. B., Len, C. N., Chen, W. N., and Lin, C. I.: Lidar observation of the cirrus cloud in the
320 tropopause at Chung Li (25°N, 121°E), *J. Atmos. Sci.*, 55, 2249– 2257, 1998.
- 321 • Noel, V., Chepfer, H., Chiriaco, M., and Yorks, J.: The diurnal cycle of cloud profiles over land
322 and ocean between 51° S and 51° N, seen by the CATS spaceborne lidar from the
323 International Space Station, *Atmos. Chem. Phys.*, 18, 9457-9473,
324 <https://doi.org/10.5194/acp-18-9457-2018>, 2018.
- 325 • Palm, S. P., Hlavka, D. L., Selmer, P., and Pauly, R.: the Cloud Aerosol Transport System (CATS)
326 Data Product Catalog release 3.0, available at: [https://cats.gsfc.nasa.gov/media/docs/CATS_](https://cats.gsfc.nasa.gov/media/docs/CATS_Data_Products_Catalog.pdf)
327 [Data_Products_Catalog.pdf](https://cats.gsfc.nasa.gov/media/docs/CATS_Data_Products_Catalog.pdf) (last access: 23 January 2018), 2016.
- 328 • Pan, L. L., and Munchak, L. A.: Relationship of Cloud Top to the Tropopause and Jet
329 Structure from CALIPSO Data, *J. Geophys. Res.*, 116, D12201,
330 <https://doi.org/10.1029/2010JD015462>, 2011.
- 331 • Pauly, R. M., Yorks, J. E., Hlavka, D. L., McGill, M. J., Amiridis, V., Palm, S. P., Rodier, S. D.,
332 Vaughan, M. A., Selmer, P. A., Kupchock, A. W., Baars, H., and Gialitaki, A.: Cloud Aerosol



- 333 Transport System (CATS) 1064 nm Calibration and Validation, *Atmos. Meas. Tech. Discuss.*,
334 <https://doi.org/10.5194/amt-2019-172>, 2019
- 335 • Pfister, L., Selkirk, H. B., Starr, D. O., Rosenlof, K., and Newman, P.A.: A meteorological
336 overview of the TC4 mission, *J. Geophys. Res.*, 115, D00J12,
337 <https://doi.org/10.1029/2009JD013316>, 2010.
- 338 • Podglajen, A., Hertzog, A., Plougonven, R., and Žagar, N.: Assessment of the accuracy of
339 (re)analyses in the equatorial lower stratosphere, *J. Geophys. Res. Atmos.*, 119, 11166–
340 11188, <https://doi.org/10.1002/2014JD021849>, 2014.
- 341 • Reichler, T., Dameris, M., and Sausen, R.: Determining the Tropopause Height from Gridded
342 Data, *Geophys. Res. Lett.*, 30, 2042, <https://doi.org/10.1029/2003GL018240>, 2003.
- 343 • Reverdy, M., Noel, V., Chepfer, H., and Legras, B.: On the origin of subvisible cirrus clouds in
344 the tropical upper troposphere, *Atmos. Chem. Phys.*, 12, 12081-12101,
345 <https://doi.org/10.5194/acp-12-12081-2012>, 2012.
- 346 • Schoeberl, M. R., Jensen, E. J., Pfister, L., Ueyama, R., Wang, T., Selkirk, H., et al.: Water
347 vapor, clouds, and saturation in the tropical tropopause layer. *J. Geophys. Res.-Atmos.*, 124,
348 3984– 4003, <https://doi.org/10.1029/2018JD029849>, 2019.
- 349 • Thomas, A., Borrmann, S., Kiemle, C., Cairo, F., Volk, M., Beuermann, J., Lepuchov, B.,
350 Santacesaria, V., Matthey, R., Rudakov, V., Yushkov, V., MacKenzie, A. R., and Stefanutti,
351 L.: In situ measurements of background aerosol and subvisible cirrus in the tropical
352 tropopause region, *J. Geophys. Res.*, 107, 4763, doi:10.1029/2001JD001385, 2002.
- 353 • Wang, T., Wu, D. L., Gong, J., and Tsai, V.: Tropopause laminar cirrus and its role in the lower
354 stratosphere total water budget. *J. Geophys. Res.-Atmos.*, 124, 7034– 7052,
355 <https://doi.org/10.1029/2018JD029845>, 2019.
- 356 • Yorks, J. E., McGill, M. J., Palm, S. P., Hlavka, D. L., Selmer, P. A., Nowottnick, E. P., Vaughan,
357 M. A., Rodier, S. D., and Hart, W. D.: An overview of the CATS level 1 processing algorithms
358 and data products, *Geophys. Res. Lett.*, 43, 4632– 4639,
359 <https://doi.org/10.1002/2016GL068006>, 2016.